Journal of Hazardous Materials 190 (2011) 652–658

Contents lists available at ScienceDirect

Journal of Hazardous Materials

journal homepage: www.elsevier.com/locate/jhazmat

Removal of anionic metals by amino-organoclay for water treatment

Young-Chul Lee, Won-Kun Park, Ji-Won Yang*

Department of Chemical and Biomolecular Engineering (BK21 Program), KAIST, 335 Gwahak-ro, Yuseong-gu, Daejeon 305-701, Republic of Korea

ARTICLE INFO

Article history:
Received 25 January 2011
Received in revised form 24 March 2011
Accepted 26 March 2011
Available online 6 April 2011

Keywords:
Organoclay
Water-soluble
Anionic metals
Humic acid
Water treatment

ABSTRACT

We describe a facile and simple one-pot synthesis of water-soluble amino-organoclay under ambient conditions. The clay was used to successfully remove environmentally toxic anionic metals, such as arsenate, chromate, and ferricyanide. The electrostatic interactions between the anionic metals and the protonated amino (ammonium) groups of the amino-organoclay resulted in rapid precipitation, within 3 min, with a high removal capacity. The maximum removal capacities (in units of mg metal per g organoclay) of the amino-organoclay clay toward $HAsO_4^{2-}$, CrO_4^{2-}, or $Fe(CN)_6^{3-}$ were, 30.73 mg/g, 34.67 mg/g, or 218.88 mg/g in case of 0.02 g, 0.03 g, and 0.005 g of the amino-organoclay, respectively. The removal efficiencies of 0.07 g, 0.09 g, and 0.03 g of the amino-organoclay whose dosage of clay was at the highest removal efficiency (%) for arsenate, chromate, and ferricyanide, respectively, presented 59.79%, 89.54%, and 97.43%. Furthermore, humic acid that ubiquitous in the organic matter present in water or soil environments, inhibited the removal rate of anionic metals, and thus the removal efficiencies toward all anionic metals were markedly reduced. Humic acid preferentially precipitated with the interaction of amino-organoclay prior to the anionic metals.

1. Introduction

Scientific and technological advances relating to water treatment are important in environmental and engineering research, which has been tasked over the last several decades with designing methods for producing safe drinking water throughout the world [1]. Among the contaminants present in (ground)water are arsenate and chromate oxyanions, which are toxic inorganic pollutants sequestered at 226 and 306 Superfund sites, respectively [2–5]. These oxyanions, which make their way into aquifers as a result of anthropogenic activities, are toxic and carcinogenic in humans, even at low doses [5]. The ferricyanide anion is frequently used as a cathode electrolyte [6] and is a source of cyanide. Similarly ferricyanide is unstable and toxic also [7,8].

Several researchers have suggested using physical adsorption methods to remove these anionic pollutants from water reservoirs. For example, nanoparticles (zero-valent iron, malachite particles, titanium oxide, etc.) [9–11], activated carbon [12], red mud [13], hydrotalcites [14], and biosorbents [15], and one of works has mainly focused on taking advantage of the negatively charged surface of naturally occurring clays, which presents a charge opposite that of the metal cations. These clays, however, cannot efficiently remove hydrophobic organic compounds or anionic pollutants. In order to apply to remove negatively charged pollutants, as an example, cationic surfactant-modified clay minerals (*i.e.*, conventional organoclays) have been developed as low-cost materials for removing organic pollutants and anionic dyes [16,17]. The monomers of cationic surfactants intercalate among the interlamellar layers to create a dual-functioning surface having hydrophobic [18–20] and positively charged properties [21–29]. Along with environmental applications of organoclays, clay-based cationic dye complexes that can remove anionic contaminants have also been reported [30,31]. As a result, organoclays were evaluated for their ability to adsorb inorganic oxyanions. However, their removal capacity was found to be low, and success was only gained by modifying the natural clays with surfactants [32,33]. The oxyanions were adsorbed onto surface sites of positive surfactant monomer surface of clay.

The desire to overcome these limitations has inspired further research into the development of easily prepared cationic organoclays for the removal of anionic contaminants from water. Layered inorganic–organic hybrid materials have been used in various applications, such as ion exchange, catalyst support, and as templates for the nanoscale assembly of hybrid materials. Recently, Mann and co-workers synthesized aminopropyl-functionalized magnesium phyllosilicate, a member of 2:1 trioctahedral phyllosilicates, *i.e.*, an amino-organoclay (hereafter abbreviated Mg clay) [34–36] that was similar to natural talc [$Si_8Mg_6O_{20}(OH)_4$]. Since 1997, Mg clay has been used as a host matrix for biomolecules [37,38] such as negatively charged lipids [39], DNA [40], enzymes [41,42], bacteriorhodopsin [43], metal stabilizers [44], and chelating linkers [45]. Very recently, further biological uses of the Mg clay along with drug nanocomposites have been tested as drug deliv-

* Corresponding author. Tel.: +82 42 350 3924; fax: +82 42 350 3910.
E-mail addresses: jiwonyang@kaist.ac.kr, jwyang@kaist.ac.kr (J.-W. Yang).

0304-3894/$ – see front matter.
doi:10.1016/j.jhazmat.2011.03.093

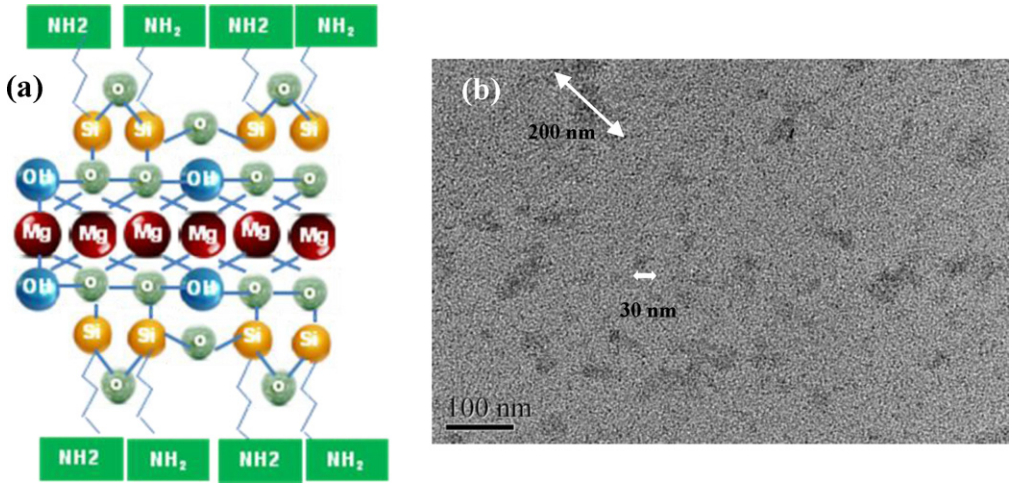

Fig. 1. Basic unit cell structure of Mg clay (a) and TEM image of Mg clay sheets in aqueous media (b).

ery systems [46] and labeled fluorescent dyes for cellular uptake [47]. However, Mg clay has not been extensively tested for use in environmental remediation applications. Here, we report, for the first time, that Mg clay can act as an adsorbent for the removal of anionic contaminants, such as arsenate, chromate, or ferricyanide, from water. The Mg clay precipitated rapidly upon complexing with the target anionic pollutants. In detail, protonated/non-protonated amino groups of Mg clay sheets are able to wrap oxyanions due to electrostatic interaction, expecting in higher removal capacity and fast precipitation. The interlayer expansion within the precipitate was measured as an indicator of the interactions by reassembling of the organo-building blocks of the Mg clay with the anionic contaminants. As a result, the pollutants were found to be uniformly distributed in the precipitated Mg clay nanoadsorbent.

The goal of this work was to synthesize and characterize Mg clay, which is cationic (due to the presence of ammonium moieties) and water-soluble. The Mg clay was used to remove anionic metals from single-solute solutions as well as from solutions containing both the metal and humic acid (hereafter denoted as HA).

2. Experimental

2.1. Chemicals

3-Aminopropyltriethoxysilane (APTES, 99%), the sodium salt of arsenate heptahydrate, chromate, HA, and $K_3Fe(CN)_6$ (>99%) were purchased from Sigma-Aldrich (St. Louis, MO, USA). Ethanol (>99.9%) was purchased from Merck KGaA (Darmstadt, Germany). Magnesium chloride hexahydrate (98.0%) was obtained from Junsei Chemical Co., Ltd. (Tokyo, Japan).

2.2. Synthesis of Mg clay

The synthesis of Mg clay was followed the literatures [35–37]: Mg clay was prepared at room temperature by the dropwise addition of APTES (2.6 mL, 11.26 mmol) to a solution of magnesium chloride (1.68 g, 17.64 mmol) in ethanol (40 g). The resulting white slurry was stirred overnight. The precipitate was isolated by centrifugation, washed with ethanol (100 mL) twice to remove excess magnesium chloride, and dried at 40 °C. The molar ratio of Mg to Si was approximately 0.75.

2.3. Characterization

Morphological characterization of the Mg clay was performed by transmission electron microscopy (TEM; JEM-2100F, JEOL LTD) with energy dispersive X-ray (EDX) analysis. The samples for TEM observation were dispersed in ddH_2O for 5 min sonication, and then dispersions was dropped onto a carbon-coated copper grid, followed by drying for overnight before injecting into the microscopy holder. Powder X-ray diffraction (PXRD) patterns were obtained on a Rigaku D/max IIIC (3 kW) with a θ/θ goniometer and a Cu Kα radiation generator operated at 40 kV, 45 mA. The scan range was 3° to 65°, and the scan rate was 1.2° 2θ/min with a step size of 0.01. Each of the clay powders (about 1 g), which was prepared with mechanical mortar, was put in the holder evenly. Fourier transform infrared (FTIR) spectra of KBr pellets (FTIR 4100, Jasco, Japan) were collected from 4000 cm^{-1} to 400 cm^{-1}. Each spectrum was calculated as the average of 32 scans with a resolution of 4 cm^{-1}. The pellet disks were prepared to be composed of 10% clay powder and 90% KBr by weight. Zeta potential measurements for the nanoadsorbents in an aqueous solution (1.5 mg/mL) were conducted using a Malvern Zetasizer Nano-ZS particle analyzer. The pH was determined using an Orion pH meter (Thermo Orion, model 710, USA). Double-distilled deionized water (>18 mΩ, ddH_2O) was used through all experiments.

2.4. Anionic metal removal capacity (q) and removal kinetics

Glass vials containing 20 mL of the 100 mg/L stock arsenic, chromate, and ferricyanide solutions, were prepared with 0.01 g Mg clay, respectively. At each sampling time, the supernatants of centrifuged arsenic and chromate samples were analyzed by inductively coupled plasma optical emission spectrometry (ICP-OES, Varian 720-ES, USA). The supernatants of the ferricyanide samples were monitored by UV–vis absorption spectroscopy (Optizen 3220UV, Mecasys, Korea) at a wavelength of 420 nm. The removal capacity (q, mg/g) and removal efficiency (%) were calculated according to

$$(C_0 - C_s) \times \frac{V}{m} = q\,(\mathrm{mg/g}) \quad \text{and} \quad \frac{C_0 - C_s}{C_0} \times 100 = (\%)$$

where C_0 and C_s represent the initial and supernatant concentrations, respectively, V is the sample volume (mL), and m is the mass (g) of the Mg clay present in solution.

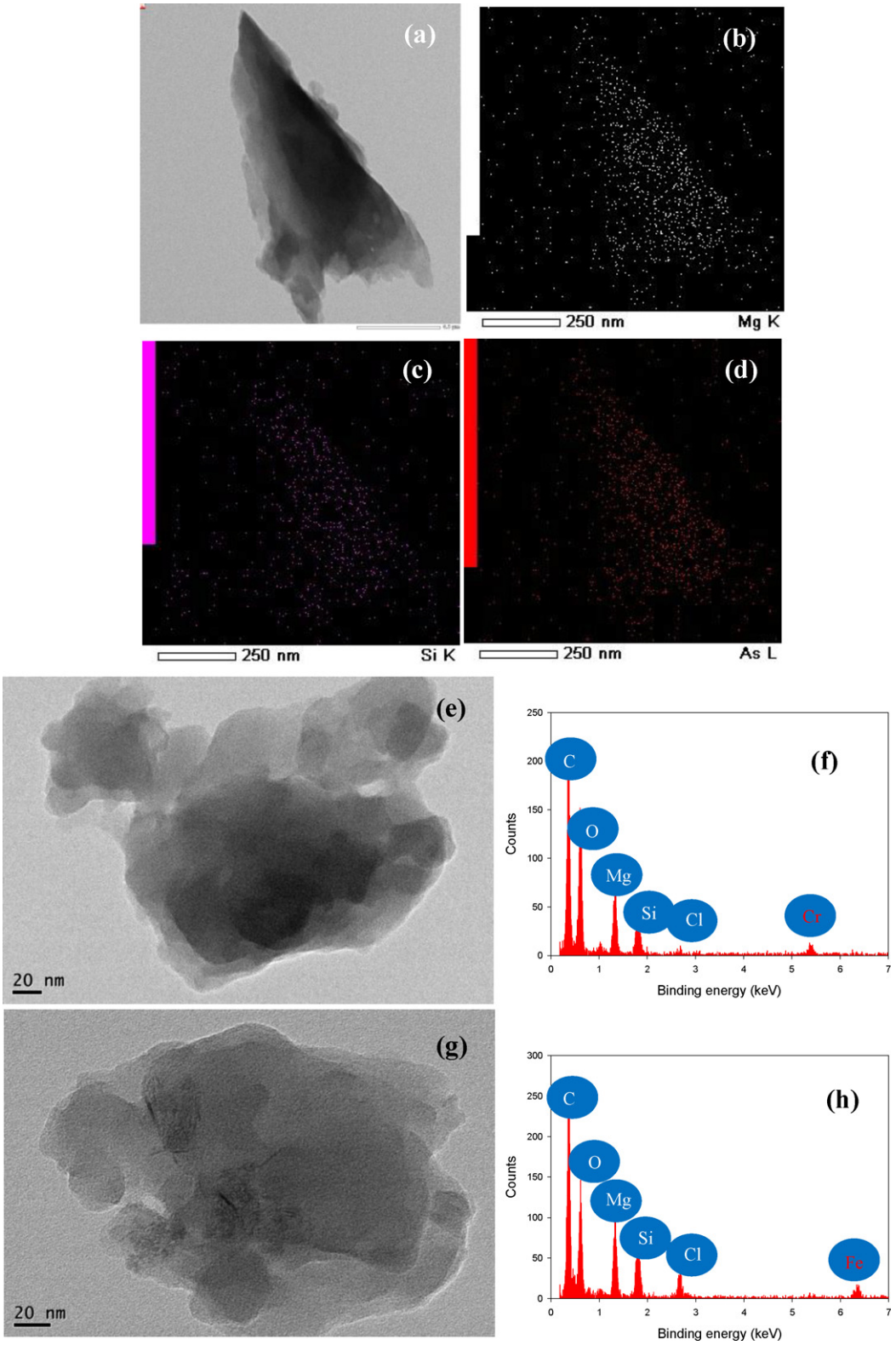

Fig. 2. STEM mapping of the Mg clay precipitated with $HAsO_4^{2-}$ (a). Elemental composition images: Mg (b), Si (c), and As (d). TEM images of the Mg clay precipitated with CrO_4^{2-} (e) and $Fe(CN)_6^{3-}$ (g). Elemental analyses corresponding to image (e) and (g) are shown in (f) and (h), respectively.

The influence of HA on the removal efficiency and rate was assessed quantitatively by UV–vis spectroscopy at 254 nm, correcting for the absorbance peaks of arsenic, chromate, and ferricyanide [49]. The removal kinetics were measured by measuring the removal rate as a function of the mass of Mg clay present in solution, 0.02 g, 0.03 g, or 0.005 g Mg clay for arsenate, chromate, and ferricyanide, respectively in which the removal kinetics was determined for arsenic, chromate, and ferricyanide at each metal's maximum capacity. The reproducibility of the results was confirmed by performing all experiments in triplicate. The influence

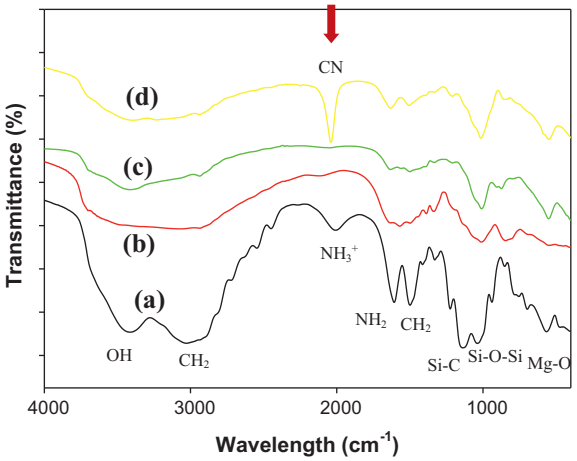

Fig. 3. FTIR spectra of Mg clay (a), Mg clay precipitated with $HAsO_4^{2-}$ (b), CrO_4^{2-} (c), and $Fe(CN)_6^{3-}$ (d).

of HA on the removal of anionic metals was measured by mixing a 100 mg/L HA stock solution in ddH_2O with each anionic metal solution to form a solution containing 25 mg/L HA and 25 mg/L anionic metal. This solution was used to measure the removal kinetics in the presence of 0.03 g Mg clay, as described above.

2.5. Species diagram of the anionic metals

The stability of pentavalent arsenic species depends on pH, and the most stable species are as follows: H_3AsO_4 (pH 0–2), $H_2AsO_4^-$ (pH 3–6), $HAsO_4^{2-}$ (pH 7–11), and AsO_4^{3-} (pH 12–14) [3]. The most stable chromate species at each pH are as follows: H_2CrO_4 (pH 0–1), $HCrO_4^-/Cr_2O_7^{2-}$ (pH 2–7), and CrO_4^{2-} (pH 8–14). The most stable ferricyanide species at each pH are as follows: HCN (aq) (pH 0–5), $Fe(CN)_6^{3-}$ (pH 6–11), and CN^- (pH 12–14). The species distributions of arsenate, chromate, and ferricyanide as a function of pH were calculated using Minteq (version 2.6), assuming a 100 mg/L aqueous solution. The predominant arsenate, chromate, and ferricyanide species at pH 9.8, which is the pH of the Mg clay solution, were $HAsO_4^{2-}$, CrO_4^{2-}, and $Fe(CN)_6^{3-}$.

3. Results and discussion

3.1. Fundamental properties of Mg clay

The synthesized Mg clay was perfectly exfoliated due to the electrostatic repulsions among the protonated amine groups. Therefore, the organo-building blocks of the Mg clay were optically transparent and water-soluble [44,47]. Fig. 1a shows the approximate unit cell composition of the Mg clay, $[H_2N(CH_2)_3]_8Mg_6Si_8O_{16}(OH)_4$ [34,35]. Upon addition of water, the pH increased within 5 min of sonication to pH 9.8 due to spontaneous protonation of $-NH_2$ groups. In other words, the Mg clay was characterized as ammonium clay in the aqueous medium, and the cationic organo-building blocks were dispersed due to the presence of the protonated amine groups [37]. The charge of the clay surface was examined by measuring the zeta potentials of the Mg clay at 1.5 mg/mL and pH 10, which were determined to be +19.6 (±0.6) mV, respectively. This findings also suggest that the positive charge on the Mg clay resulted from protonation of the aminopropyl $[NH_3^+(CH_2)_3-]$ functionalities attached to the inorganic framework.

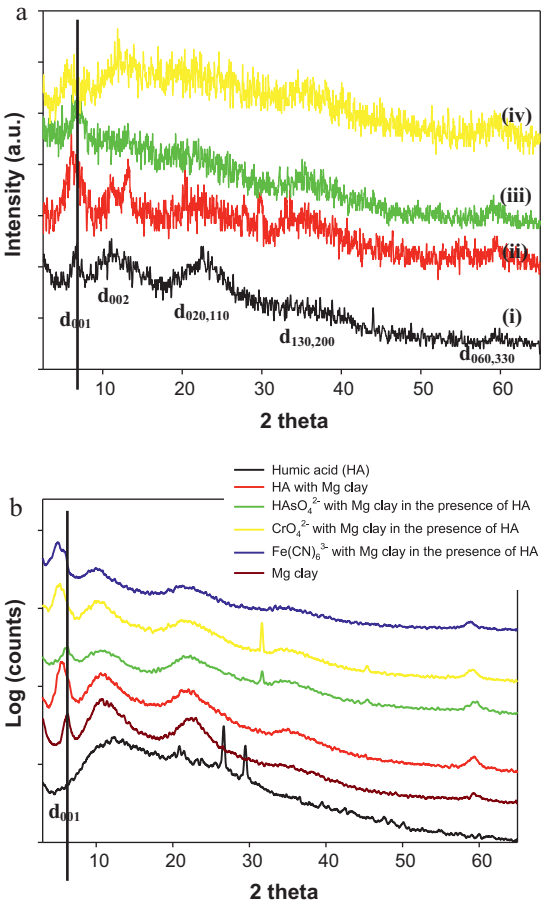

Fig. 4. PXRD patterns (a) of Mg clay (i), Mg clay precipitated with $HAsO_4^{2-}$ (ii), CrO_4^{2-} (iii), and $Fe(CN)_6^{3-}$ (iv). PXRD patterns (b) of Mg clay precipitated with anionic metals in the presence of HA.

3.2. TEM observation

The size of the exfoliated Mg clay ranged from 30 to 200 nm in the TEM image (Fig. 1b), in agreement with the results from previous studies [35–37]. The microstructures of the anionic contaminant-assembled Mg clay composites were also observed by TEM (Fig. 2). Micrographs of the precipitates revealed typical plate-shaped particles, and the sample images revealed a layered structure with typical clay sheet edges (Fig. 2a, e, and g). Scanning transmission electron microscopy (STEM) analysis of the precipitate materials indicated the presence of Mg, Si, and As in the precipitate of the $HAsO_4^{2-}$ with Mg clay (Fig. 2b–d). EDX analysis revealed the presence of Cr and Fe in the precipitated Mg clay material (Fig. 2f and h). The presence of Cl ions is the stabilized cationic amine groups of AMP clay. The layered structures of the anionic contaminants-Mg clay material were observed by TEM, which showed flake-like particles and uniformly distributed species. However, when considering intense peaks of the interlayer spacing were observed in the XRD pattern, it indicates that the electrostatic interactions between the Mg clay and the anionic contaminants created well-ordered stacking of the exfoliated Mg clay sheets.

3.3. FTIR spectra

The FTIR spectra of the Mg clay contained peaks that corresponded to the following functional groups: OH (3384 cm^{-1}), CH_2 peak (3000 cm^{-1}), NH_3^+ (2007 cm^{-1}), NH_2 (1607 cm^{-1}), Si–C

Table 1
Basal spacing values of precipitate of Mg clay with anionic species and HA.

Sample	$d_{(001)}$ spacing/Å
Mg clay	14.1
Mg clay/$HAsO_4^{2-}$	15.5
Mg clay/CrO_4^{2-}	14.6
Mg clay/$Fe(CN)_6^{3-}$	17.2
Mg clay/HA	15.8
HA	–
Mg clay/$HAsO_4^{2-}$/HA	14.1
Mg clay/CrO_4^{2-}/HA	17.2
Mg clay/$Fe(CN)_6^{3-}$/HA	17.5

(1144 cm^{-1}), Si–O–Si (1130 cm^{-1}), Si–OH (1034 cm^{-1}), Mg–O–Si (849 cm^{-1}), Si–O–C (849 cm^{-1}), and Mg–O (559 cm^{-1}) (Fig. 3a) [34–39]. All CH_2 peak (3000 cm^{-1}) vibrations of precipitated Mg clay with anionic metals were broadened and weakened (Fig. 3b–d). The NH_3^+ peak (2007 cm^{-1}) disappeared in the samples containing the precipitated Mg clay with anionic contaminants due to interactions between the cationic $-NH_3^+$ group and the anionic contaminants [40,46,47]. Therefore, organo-functional groups with flexible [$NH_2(CH_2)_3-$] were interacted with oxyanions. The precipitated Mg clay with ferricyanide indicated that the intense peak at 2039 cm^{-1} was originated from a CN stretching mode with marked brown arrow (Fig. 3d).

3.4. PXRD patterns

The powder X-ray diffraction (PXRD) patterns of the Mg clay in Fig. 4a (i) showed an interlayer reflection corresponding to a d_{001} spacing of 1.41 nm and the characteristics of the intra-plane d_{060} smectite reflection at $2 = 59^\circ$, which agreed well with previous reports [47]. The PXRD patterns revealed sharp and intense peaks, corresponding to a slight expansion in the d_{001} basal spacing due to complex formation with the anionic metals and the organo-building sheets dispersion of the Mg clay. The samples retained the characteristic d_{060} smectite reflection at $2\theta = 59^\circ$, corresponding to a higher angle peak. Fig. 4a (ii–iv) show that the basal spacings (Å) of the Mg clay precipitate bound to $HAsO_4^{2-}$, CrO_4^{2-}, and $Fe(CN)_6^{3-}$ were 15.5 Å, 14.6 Å, and 17.2 Å. Considering the sizes of each ionic guest species, $HAsO_4^{2-}$ (3.35 Å), CrO_4^{2-}(2.40 Å), and $Fe(CN)_6^{3-}$ (8.00 Å), anionic metals were intercalated into the Mg clay galleries, and then interlayer space were shrunk compactly by the precipitates. As depicted in Fig. 4b, the precipitate containing Mg clay and HA showed a d_{001} spacing of 15.8 Å, indicating that bulky macromolecule HA sterically hindered the reassembly of the Mg clay sheets. Flocculated precipitates formed. Larger anionic species tend to exert stronger steric effects, which was induced by the difference of molecule size. The steric effect may be evidence for a slight increase in the interlayer spacing and correspond to degree of interlayer distance expansion by 1.4 Å, 0.5 Å, and 3.1 Å,

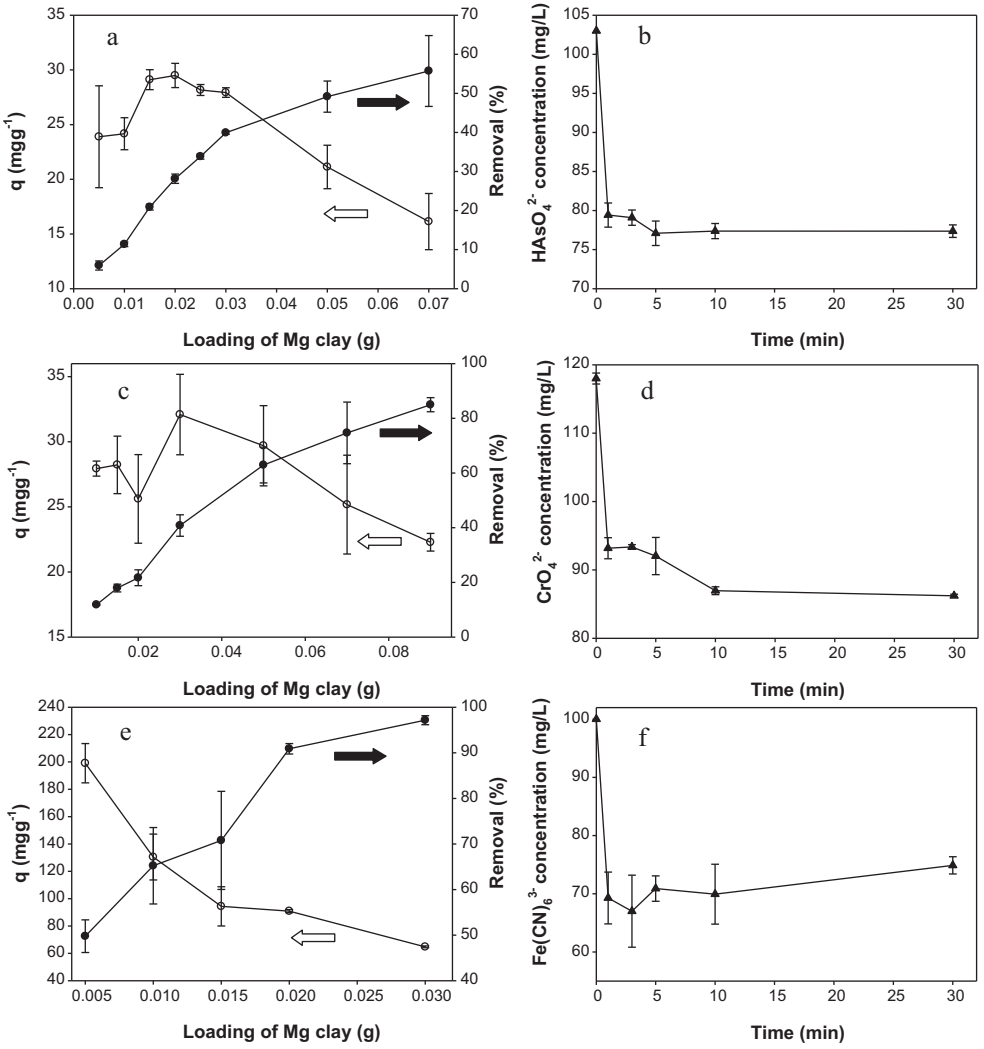

Fig. 5. Removal capacities (q) and efficiencies for $HAsO_4^{2-}$ (a), CrO_4^{2-} (c), and $Fe(CN)_6^{3-}$ (e). Removal kinetics for $HAsO_4^{2-}$ (b), CrO_4^{2-} (d), and $Fe(CN)_6^{3-}$ (f).

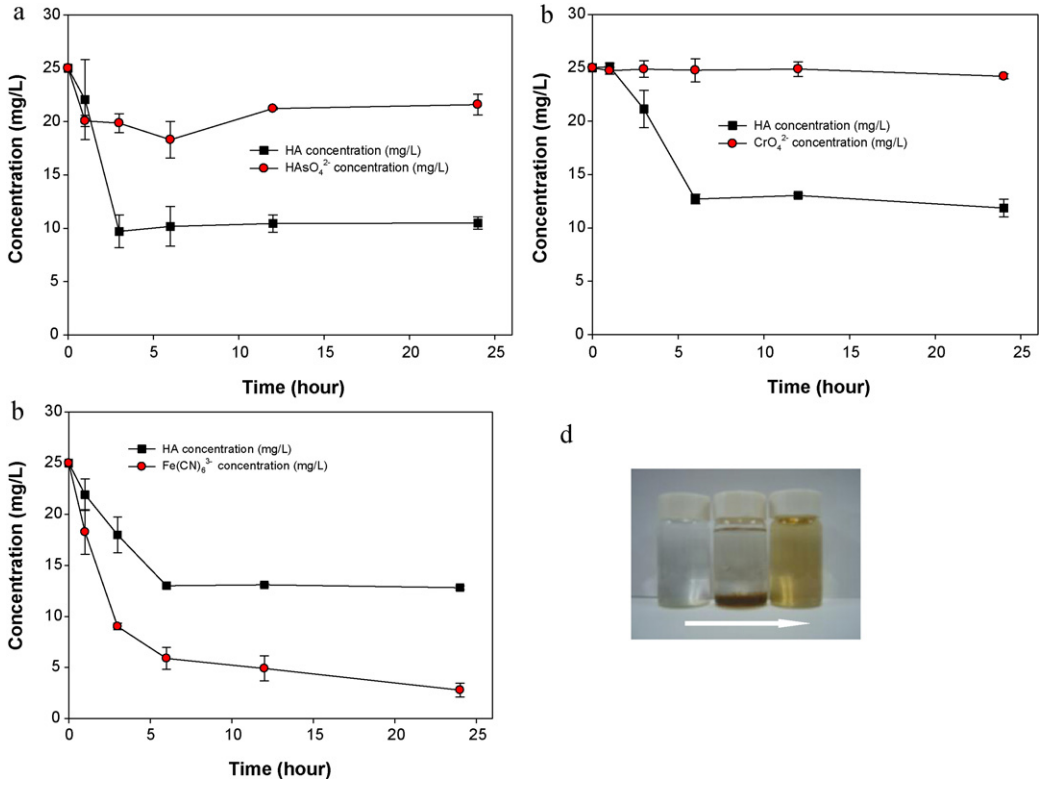

Fig. 6. The kinetics of $HAsO_4^{2-}$ (a), CrO_4^{2-} (b), and $Fe(CN)_6^{3-}$ (c) in the presence of HA. The photographs of Mg clay, Mg clay with HA, and HA in aqueous solution from left to right vial images (d).

for $HAsO_4^{2-}$, CrO_4^{2-}, and $Fe(CN)_6^{3-}$, respectively. The increase in the basal spacings was proportional to the ionic size of the contaminants. Interestingly, the presence of HA did not affect the d_{001} spacings of the reassembled Mg clay sheets bound to $HAsO_4^{2-}$. In contrast, CrO_4^{2-} and $Fe(CN)_6^{3-}$ displayed a slight increase in the basal spacings due to the strong interactions between HA and the Mg clay (Table 1). Therefore, intercalation of the anionic metals into the Mg clay interstices was inhibited in the presence of HA.

3.5. Mg clay removal of the anionic metals in a single-solute system

The removal capacities (q, mg/g) of the organo-building blocks of Mg clay toward the anionic metals were inversely proportional to the valency of the negative charge (Fig. 5a, c, and e). Ferricyanide yielded a maximum removal capacity at a clay dose (mass) that was lower than those of arsenic and chromate. The total removal efficiency (%) increased for all contaminants as the Mg clay dosage increased. The maximum removal efficiencies at their corresponding Mg clay dosages were $59.79 \pm 3.24\%$ at 0.07 g for arsenic, $89.54 \pm 4.35\%$ at 0.09 g for chromate, and $97.43 \pm 1.08\%$ at 0.03 g for ferricyanide under identical conditions with concentration and volume metal ions solution. Further increases in the Mg clay dosage increased the removal efficiencies achieved to approximately 100% (data not shown). The electrostatic interactions between the positively charged aminopropyl pendant groups of the Mg clay and the polar anionic ions drove the adsorption of metals by the clay. The removal kinetics studies (Fig. 5b, d, and f) revealed rapid aggregation of the anionic contaminants and the Mg clay, which immediately precipitated. The reaction reached completion within 3 min, and equilibrium was achieved in approximately 10 min. Water treatment processes require fast removal kinetics to minimize treatment costs.

3.6. Effect of HA on the Mg clay removal of anionic metals

As shown in Fig. 6, we tested the removal of anionic metals in the presence of HA, which is a representative natural organic material present in natural aquifers and water supplies [48,49]. HA was found to be removed by precipitation during the first 5 min. Fig. 6d exhibited photographs of Mg clay and Mg clay with HA, and only HA in aqueous solution from left to right vial image. Precipitation of Mg clay with HA could be easily observed by naked eyes. However, no more HA removed below 14 mg/L concentration of HA in all experiments as time elapsed. Moreover, removal of both arsenate and chromate was not observed, indicating that HA significantly inhibited the removal of these pollutants (Fig. 6a and b). Ferricyanide, on the other hand, was removed in the presence of HA once most of the HA had been removed. Ferricyanide was then gradually removed over time, possibly due to the strong electrostatic attraction between the trivalent $Fe(CN)_6^{3-}$ and the Mg clay sheets (Fig. 6c). The other side, arsenate and chromate were found to be removed at higher Mg clay dosages: 0.05 g, 0.07 g, and 1 g of Mg clay (data not shown). These findings indicate that the removal efficiency is significantly affected by steric hindrance of bulky macromolecules of HA when they interacted with dispersions of Mg clay sheets, rather than by electrostatic attraction between arsenate or chromate and the Mg clay.

4. Conclusion

In summary, we have demonstrated a facile one-pot synthesis of Mg clay for use as a novel nanoadsorbent for the removal of anionic contaminants from water. The cationic Mg clay easily precipitated due to induced electrostatic interactions between the arsenate, chromate, or ferricyanide with the Mg clay. The clay also showed high removal capacities. Solutions containing HA displayed limited

removal, possibly due to steric hindrance during the reassembly of exfoliated Mg clay sheets. Initially, HA was removed by the Mg clay, and the anionic species were removed later, for example, upon addition of more Mg clay. It is anticipated that cationic Mg clay presents a new material for use in the removal of a variety of anionic pollutants which removal adsorbents had been limited to natural clay or cationic surfactant-modified clays.

Acknowledgments

This subject is supported by Korea Ministry of Environment as "Converging technology project". We thank all members of the National NanoFab Center (NNFC) for fruitful discussions about TEM and SEM imaging.

References

[1] M.A. Shannon, P.W. Bohn, M. Elimelech, J.G. Georgiadis, B.J. Mariñas, A.M. Mayes, Science and technology for water purification in the coming decades, Nature 452 (2008) 301–310.
[2] J.-Q. Jiang, Removal arsenic from groundwater for the developing world—a review, Water Sci. Technol. 44 (2001) 89–98.
[3] J. Iqbal, H.-J. Kim, J.-S. Yang, K. Baek, J.-W. Yang, Removal of arsenic from groundwater by micellar-enhanced ultrafiltration (MEUF), Chemosphere 66 (2007) 970–976.
[4] M. Costa, Potential hazards of hexavalent chromate in our drinking water, Toxicol. Appl. Pharmacol. 188 (2003) 1–5.
[5] S. Fendorf, M.J. Eick, P. Grossl, D.L. Sparks, Arsenate and chromate retention mechanisms on goethite. 1. Surface structure, Environ. Sci. Technol. 31 (1997) 315–320.
[6] Z. Ren, T.E. Ward, J.M. Regan, Electricity production from cellulose in a microbial fuel cell using a defined binary culture, Environ. Sci. Technol. 41 (2007) 4781–4786.
[7] T.L. Theis, R. Iyer, L.W. Kaul, Kinetic studies of cadmium and ferricyanide adsorption on goethite, Environ. Sci. Technol. 22 (1988) 1013–1017.
[8] H.-J. Hong, H. Kim, K. Baek, J.-W. Yang, Removal of arsenate, chromate and ferricyanide by cationic surfactant modified powdered activated carbon, Desalination 223 (2008) 221–228.
[9] A.M Giasuddin, S.R. Kanel, H. Choi, Adsorption of humic acid onto nanoscale zerovalent iron and its effect on arsenic removal, Environ. Sci. Technol. 41 (2007) 2022–2027.
[10] J. Saikia, B. Saha, G. Das, Efficient removal of chromate and arsenate from individual and mixed system by malachite nanoparticles, J. Hazard. Mater. 186 (2011) 575–582.
[11] M. Pena, X. Meng, G.P. Korfiatis, C. Jing, Adsorption mechanism of arsenic on nanocrystalline titanium dioxide, Environ. Sci. Technol. 40 (2006) 1257–1262.
[12] H.-J. Hong, H. Kim, Y.-J. Lee, J.-W. Yang, Removal of anionic contaminants by surfactant modified powdered activated carbon (SM-PAC) combined with ultrafiltration, J. Hazard. Mater. 170 (2009) 1242–1246.
[13] Y. Li, J. Wang, Z. Luan, Z. Liang, Arsenic removal from aqueous solution using ferrous based red mud sludge, J. Hazard. Mater. 177 (2010) 131–137.
[14] K.-H. Goh, T.-T. Lim, Z. Dong, Application of layered double hydroxides for removal of oxyanions: a review, Water Res. 42 (2008) 1343–1368.
[15] D. Mohan, C.U. Pittman Jr., Arsenic removal from water/wastewater using adsorbents—a critical review, J. Hazard. Mater. 142 (2007) 1–53.
[16] M. Kowalska, H. Güler, D.L. Cocke, Interactions of clay minerals with organic pollutants, Sci. Total Environ. 141 (1994) 223–240.
[17] V. Vimonses, S. Lei, B. Jin, C.W.K. Chow, C. Saint, Kinetic study and equilibrium isotherm analysis of Congo Red adsorption by clay materials, Chem. Eng. J. 148 (2009) 354–364.
[18] S.K. Dentel, J.Y. Bottero, K. Khatib, H. Demougeot, J.P. Duguet, C. Anselme, Sorption of tannic acid, phenol, and 2,4,5-trichlorophenol on organoclays, Water Res. 29 (1995) 1273–1280.
[19] S.K. Dentel, A.I. Jamrah, D.K. Sparks, Sorption and cosorption of 1,2,4-trichlorobenzene and tannic acid by organo-clays, Water Res. 32 (1998) 3689–3697.
[20] A. Khenifi, B. Zohra, B. Kahina, H. Houari, D. Zoubir, Removal of 2,4-DCP from wastewater by CTAB/bentonite using one-step and two-step methods: a comparative study, Chem. Eng. J. 146 (2009) 345–354.
[21] Y. Seki, K. Yurdakoç, Paraquat adsorption onto clays and organoclays from aqueous solution, J. Colloid Interface Sci. 287 (2005) 1–5.
[22] P. Baskaralingam, M. Pulikesi, D. Elango, V. Ramamurthi, S. Sivanesan, Adsorption of acid dye onto organobentonite, J. Hazard. Mater. B128 (2006) 138–144.
[23] A. Özcan, Ç. Ömeroğlu, Y. Erdoğan, A.S. Özcan, Modification of bentonite with a cationic surfactant: an adsorption study of textile dye Reactive Blue 19, J. Hazard. Mater. 140 (2007) 173–179.
[24] L. Zhu, J. Ma, Simultaneous removal of acid dye and cationic surfactant from water by bentonite in one-step process, Chem. Eng. J. 139 (2008) 503–509.
[25] Q. Zhou, H.P. He, J.X. Zhu, W. Shen, R.L. Frost, P. Yuan, Mechanism of *p*-nitrophenol adsorption from aqueous solution by $HDTMA^+$-pillared montmorillonite—implications for water purification, J. Hazard. Mater. 154 (2008) 1025–1032.
[26] B. Zohra, K. Aicha, S. Fatima, B. Nourredine, D. Zoubir, Adsorption of Direct Red 2 on bentonite modified by cetyltrimethylammonium bromide, Chem. Eng. J. 136 (2008) 295–305.
[27] X. Yu, C. Wei, L. Ke, Y. Hu, X. Xie, H. Wu, Development of organovermiculite-based adsorbent for removing anionic dye from aqueous solution, J. Hazard. Mater. 180 (2010) 499–507.
[28] R. Zhu, T. Wang, J. Zhu, F. Ge, P. Yuan, H. He, Structural and sorptive characteristics of the cetyltrimethylammonium and polyacrylamide modified bentonite, Chem. Eng. J. 160 (2010) 220–225.
[29] S.T. Akar, R. Uysal, Untreated clay with high adsorption capacity for effective removal of C.I. Acid Red 88 from aqueous solutions: batch and dynamic flow studies, Chem. Eng. J. 162 (2010) 591–598.
[30] M. Borisover, E.R. Graber, F. Bercovich, Z. Gerstl, Suitability of dye-clay complexes for removal of non-ionic organic compounds from aqueous solutions, Chemosphere 44 (2001) 1033–1040.
[31] G. Rytwo, Y. Kohavi, I. Botnick, Y. Gonen, Use of CV- and TPP-montmorillonite for the removal of priority pollutants from water, Appl. Clay Sci. 36 (2007) 182–190.
[32] Z. Li, R.S. Bowman, Retention of inorganic oxyanions by organo-kaolinite, Water Res. 35 (2001) 3771–3776.
[33] B. Sarkar, Y. Xi, M. Megharaj, G.S.R. Krishnamurti, D. Rajarathnam, R. Naidu, Remediation of hexavalent chromium through adsorption by bentonite based Arquad® 2HT-75 organoclays, J. Hazard. Mater. 183 (2010) 87–97.
[34] S. Mann, S.L. Burkett, S.A. Davis, C.E. Fowler, N.H. Mendelson, S.D. Sims, D. Walsh, N.T. Whilton, Sol–gel synthesis of organized matter, Chem. Mater. 9 (1997) 2300–2310.
[35] S.L. Burkett, A. Press, S. Mann, Synthesis, characterization, and reactivity of layered inorganic–organic nanocomposites based on 2:1 trioctahedral phyllosilicates, Chem. Mater. 9 (1997) 1071–1073.
[36] B. Lebeau, J. Brendlé, C. Marichal, A.J. Patil, E. Muthusamy, S. Mann, One-step synthesis and solvent-induced exfoliation of hybrid organic–inorganic phyllosilicate-like materials, J. Nanosci. Nanotechnol. 6 (2006) 352–359.
[37] A.J. Patil, S. Mann, Self-assembly of bio-inorganic nanohybrids using organoclay building blocks, J. Mater. Chem. 18 (2008) 4605–4615.
[38] S. Mann, Self-assembly and transformation of hybrid nano-objects and nanostructures under equilibrium and non-equilibrium conditions, Nat. Mater. 8 (2009) 781–792.
[39] A.J. Patil, E. Muthusamy, A.M. Seddon, S. Mann, Higher-order synthesis of organoclay pipes using self-assembled lipid templates, Adv. Mater. 15 (2003) 1816–1819.
[40] A.J. Patil, M. Li, E. Dujardin, S. Mann, Novel bioorganic nanostructures based on mesolamellar interaction or single-molecule wrapping of DNA using organoclay building blocks, Nano Lett. 7 (2007) 2660–2665.
[41] A.J. Patil, E. Muthusamy, S. Mann, Synthesis and self-assembly of organoclay wrapped biomolecules, Angew. Chem. Int. Ed. 43 (2004) 4928–4933.
[42] A.J. Patil, E. Muthusamy, S. Mann, Fabrication of functional protein-organoclay lamellar nanocomposites by biomolecules-induced assembly of exfoliated aminopropyl-functionalized magnesium phyllosilicates, J. Mater. Chem. 15 (2005) 3838–3843.
[43] K.M. Bromley, A.J. Patil, A.M. Seddon, P. Booth, S. Mann, Bio-functional mesolamellar nanocomposites based on inorganic/polymer interaction in purple membrane (Bacteriorhodopsin) films, Adv. Mater. 19 (2007) 2433–2438.
[44] K.K.R. Datta, M. Eswaramoorthy, C.N.R. Rao, Water-solubilized aminoclay-metal nanoparticle composites and their novel properties, J. Mater. Chem. 17 (2007) 613–615.
[45] I.L. Lagadic, Schiff base chelate-functionalized organoclays, Micropor. Mesopor. Mater. 95 (2006) 226–233.
[46] S.C. Holmström, A.J. Patil, M. Butler, S. Mann, Influence of polymer co-intercalation on guest release from aminopropyl-functionalized magnesium phyllosilicate mesolamellar nanocomposites, J. Mater. Chem. 17 (2007) 3894–3900.
[47] Y.-C. Lee, T.-H. Lee, H.-K. Han, W.J. Go, J.-W. Yang, H-.J. Shin, Optical properties of fluorescein-labeled organoclay, Photochem. Photobiol. 86 (2010) 520–527.
[48] A.B.M. Giasuddin, S.R. Kanel, H. Choi, Adsorption of humic acid onto nanoscale zerovalent iron and its effect on arsenic removal, Environ. Sci. Technol. 41 (2007) 2022–2027.
[49] Y.-C. Lee, C.-W. Kim, J.-Y. Lee, H.-J. Shin, J.-W. Yang, Characterization of nanoscale zero valent iron modified by nonionic surfactant for trichloroethylene removal in the presence of humic acid: a research note, Desal. Water Treat. 10 (2009) 33–38.